batteries

MDPI

Communication

Improved Mechanistic Degradation Modes Modeling of Lithium and Sodium Plating

David Beck [1], Agata Greszta [2], Alexander Roberts [2] and Matthieu Dubarry [1,*]

[1] Hawai'i Natural Energy Institute, University of Hawai'i at Mānoa, Honolulu, HI 96822, USA; dmbeck@hawaii.edu
[2] Centre for E-Mobility and Clean Growth, Coventry University, Coventry CV1 2JH, UK; ad7462@coventry.ac.uk (A.G.); ad2370@coventry.ac.uk (A.R.)
* Correspondence: matthieu@hawaii.edu

Abstract: Lithium and sodium plating are inevitable when using negative electrodes with an electrochemical potential close to one of the charge carriers. Typical testing and modeling assume that plating occurs at 0 V when measured against the charge carrier. While this might be true under thermodynamic equilibrium, this is not true outside of steady state. This has significant implications as, by taking this into account, the testing voltage window of negative electrodes could be extended to allow gathering data for more complete discharges at higher rates. Moreover, from a modeling standpoint, it could also allow us to more accurately predict plating initiation potentials dynamically. This work presents the preliminary results of the investigation of what parameters are influencing the plating potential and how to take them into account in testing and modeling.

Keywords: lithium plating; sodium plating; degradation modes mechanistic modeling

Citation: Beck, D.; Greszta, A.; Roberts, A.; Dubarry, M. Improved Mechanistic Degradation Modes Modeling of Lithium and Sodium Plating. *Batteries* **2024**, *10*, 408. https://doi.org/10.3390/batteries10120408

Academic Editors: Jian Ma, Yujie Cheng and Meiling Yue

Received: 13 October 2024
Revised: 13 November 2024
Accepted: 20 November 2024
Published: 21 November 2024

1. Introduction

Lithium plating is believed to be one of the main contributors to the degradation of commercial lithium-ion batteries, especially at low temperatures and higher rates. As such, it has been extensively studied in the literature with multiple reviews already available for both experimental and modeling work [1–8]. While some experimental studies [9,10] and models [11–15] showed that the voltage of the negative electrode (NE) could go below 0 V [16], the plating threshold is still, in most cases, considered to be at 0 V independently of the required rate. The literature on sodium plating is much scarcer, with most of the work being performed on metallic sodium electrodes [10,17–21] with no plating-specific modeling work yet, to the best of our knowledge, although several studies mentioned that a significant amount of the NE capacity was pushed under 0 V under normal utilization [16,22,23].

The modeling work by Mukherjee's group [12,13] showed the importance of considering the electrochemical response of each electrode separately to enable a deeper understanding of the plating conditions. While they used a physic-based model, a degradation modes mechanistic modeling approach could be better fitted for this task, as it excels in relating effects on each electrode without the extensive parameterization and calculation cost required in other models. The approach has gained tremendous attention since its inception in the mid to late 2000s, with seminal work by Bloom et al. [24,25], Honkura et al. [26], Dahn et al. [27], and ourselves [28]. This modeling framework relies on the matching of half-cell data of each electrode to emulate the full-cell response of the cells. Changing the matching of the electrodes allows to simulate the impact of different degradation modes [28,29] and thus provide insights into cell degradation. Our group introduced the first mechanistic degradation modes model that was able to perform emulations at different rates but also account for plating by considering the NE as a blend between the active material and the metallic charge carrier [28]. This enabled to predict the apparition of knees [30] and to define a new parameter, the plating threshold, that allowed to determine

when conditions are favorable for plating [31], i.e., when there is not enough NE remaining to intercalate the lithium from the positive electrode (PE) or when its resistance pushes its potential below the plating potential [32,33].

Our approach could still be enhanced, most notably by allowing more accurate plating potential simulations and by increasing the testing range for the half-cell data. For the former, the model currently assumes a constant potential of 0 V for the metallic phase of the charge carrier while the literature showed that this is not the case outside of the steady state, especially for higher rates [9,10]. There is, therefore, a need for a new parameter to be integrated into the modeling framework to account for these potential variations. For the latter, the cutoff voltage for experimental laboratory testing of NE at the end of discharge is typically set to be above 0 V to avoid any possible plating. This has two implications; first, there will be a drop of potential on the NE in the simulations (increase on the full cell) with a discontinuity when the lithiation of the NE is completed and plating initiates, * in Figure 1a, because no data are available in between the cutoff voltage and the plating potential. Second, some discharges at higher rates will not be completed because the half-cell higher polarization, compared to full cells, will be pushing more capacity below the cutoff and thus outside of the potential window, as shown in Figure 1b. As a result, some capacity accessible by the full cell will be missing from the simulation, and plating will be predicted way earlier than it should, as shown in Figure 1a. This could be avoided by introducing negative cutoff voltages for the graphite at rates away from equilibrium, similar to what was proposed by Verbrugge et al. in 1997 [34].

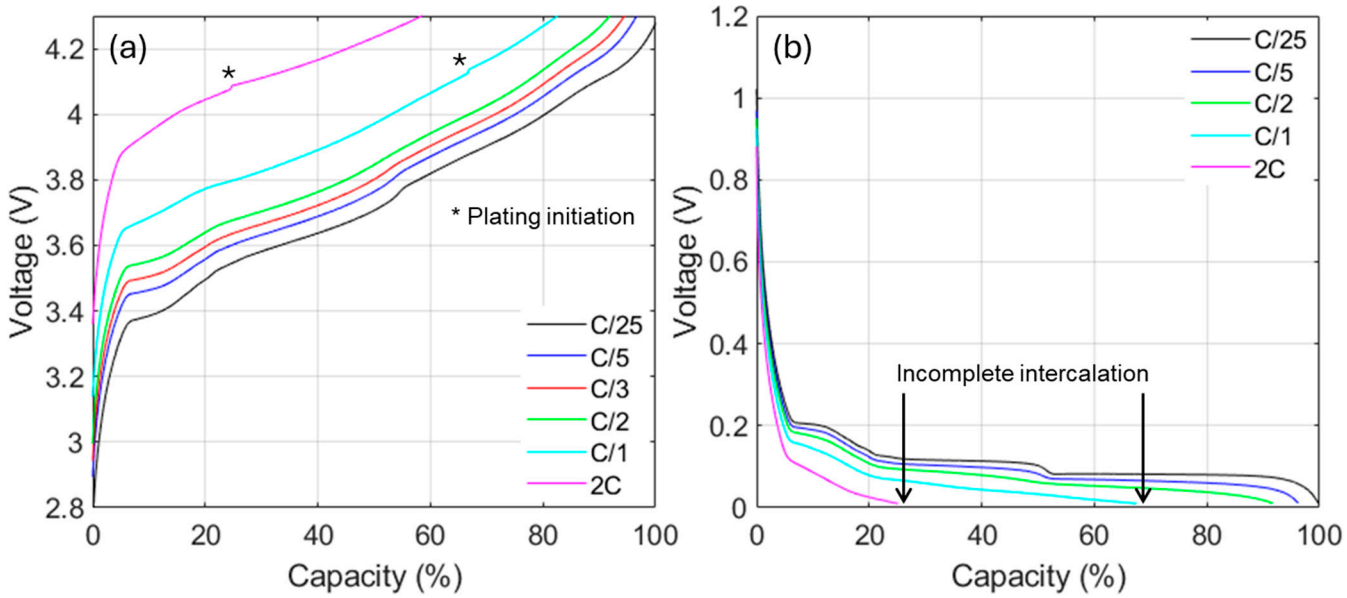

Figure 1. (**a**) Example of a graphite/lithium nickel–cobalt–aluminum oxide full-cell charging emulation at different rates showcasing the predicted lithium plating onsets (*). The simulations were performed using the alawa toolbox [28,35] using stock materials, a loading ratio of 1.2, and an offset of 2%. (**b**) Associated NE lithiation half-cell data used for the simulations.

Ultimately, we aim to propose both a new half-cell reference performance test (RPT) protocol ensuring that the maximum information is extracted from the half-cell testing by introducing a rate-dependent end of discharge cutoff voltage, and a better implementation of the plating potential in the model with the addition of a new parameter in the mechanistic degradation modes modeling framework, the plating resistance. As this resistance could potentially be dependent on chemistry, electrolyte, architecture, and temperature, among others, significant experimental validation is needed before a general understanding can be deciphered and discussed. This work presents some preliminary results from our investigation of these issues.

2. Materials and Methods

In this work, 0.9 cm and 1.6 cm diameter circular electrodes were prepared and tested in Hawaii. The electrodes were punched out of a sheet of NE harvested from commercial Li-ion and Na-ion cells. A portion of the electrode sheet was first rinsed using dimethyl carbonate before one side was cleaned using N-Methylpyrrolidone. Electrodes were then cut into 0.9 cm with a punch and into 1.6 cm diameter disks using an EL-CUT punching tool (EL-CELL, Hamburg, Germany) before being assembled in a Swagelok and 2032 coin cells, respectively, with an NE consisting of metallic lithium or sodium, one glass fiber GF/A separator (EL-CELL, Hamburg, Germany), and an electrolyte made of ethylene and propylene carbonates (EC and PC respectively) in a 50:50 ratio with 1M $LiPF_6$ for the lithium cells and 1 M $NaClO_4$ for the sodium cells. All the chemicals were obtained from Sigma Aldrich (St. Louis, MO, USA), and all the experiments were performed on a VMP3 potentiostat/galvanostat (Biologic, Claix, France).

In addition to the 0.9 and 1.5 cm electrodes, 35 cm^2 electrodes were prepared and tested in the United Kingdom. The electrodes were coated and calendered in house on a reverse comma bar coater and heated calendar (both MTI Corporation, Richmond, CA, USA) to areal loadings of 1.1 and 3.3 mAh cm^{-2} and a density of 1.6 g cm^{-3}. The electrodes were cut using a die cutter (MTI Corporation, USA) to a 7 × 5 cm rectangle with an uncoated flag for tab welding. The electrodes were assembled into single-layer pouch cells with a double-sided lithium metal on copper electrode (50 um per side on 12 um copper, Cambridge Energy Solutions, Cambridge, UK) with a trilayer polymeric separator (Celgard H1609) and an electrolyte of 1 M $LiPF_6$ in EC/ethyl methyl carbonate (EMC) 3:7 with 2% vinylene carbonate. All pouch cell assembly was performed in an argon glovebox with water and oxygen <1 ppm.

All the plating experiments were subjected to the same electrochemical cycling with C/50, C/25, C/16, C/8, C/4, C/2, and C/1 cycles with 4 h rests at the end of the charge and discharge. The charge cutoff was set to 1.2 V at the end of the charge. A residual capacity step at C/50 followed by another 4 h rest was performed at the end of each charge to ensure discharges start from a similar state [36]. The discharge cutoffs were not voltage based but capacity based, with the cutoff set to 130% of the nominal capacity to allow for significant plating.

A modified RPT experiment was performed using a 1.6 cm diameter electrode with the same electrolyte and separators as above. Full cycles were performed at C/50, C/25, C/16, C/8, C/4, C/2, C/1, 2C, and 4C with 4 h rests at the end of charge and discharge. The cutoffs were set to 1.2 V at the end of the charge and were 0 mV, −5 mV, −10 mV, −15 mV, −25 mV, −45 mV, −60 mV, and −115 mV in discharge, respectively to the rates. A residual capacity step at C/50 followed by another 4 h rest was performed at the end of each regime.

All the simulations were performed using the alawa toolbox [28,33,35] using a stock lithium nickel–cobalt–aluminum oxide for the PE and either a stock graphite or the graphite data obtained from the RPT with variable cutoffs. The loading ratio was set at 1.2 and the offset to 2%. As described in [28], the full-cell data were calculated by subtracting the rate-dependent NE responses from the rate-dependent PEs after they were scaled from the loading ratio and shifted by the offset. Responses at different rates were obtained using a 2D interpolation within the available rates for the selected materials. Plating was simulated by considering the NE to be a blend of graphite and metallic lithium [28,33]. For this work, a new parameter, the plating resistance, was added to the toolbox to enable variable plating potentials as a function of the rate. In Figure 1, the plating resistance was set to 0 to simulate the old approach in which the plating potential is rate independent at 0 V.

3. Results and Discussion

First, it was important to verify that the plating initiation potential is rate dependent. Figure 2a presents an experiment on a 1.6 cm^2 graphite electrode vs. a metallic lithium counter electrode for which the cutoff at the end of discharge was set to 130% of the nominal

capacity. Because the cutoff was set to be lower than typical for a graphite cell, some lithium plated. The observed response for the plating was in accordance with the literature [9,37,38], with a local minima reached before a stabilized potential that is slightly higher, followed by another drop that could be related to dead lithium, as reported by Wood et al. [39]. The plating and stripping potentials, measured as the maximum after the first local minimum is reached in discharge and the opposite in charge, were rate dependent, as shown in Figure 2b, symmetric, and had their absolute value increase linearly with the rate and a resistance of about 10 mΩ or 0.1 Ω Ah when normalized to the rate. This resistance will be referred to as the plating resistance in the rest of this work.

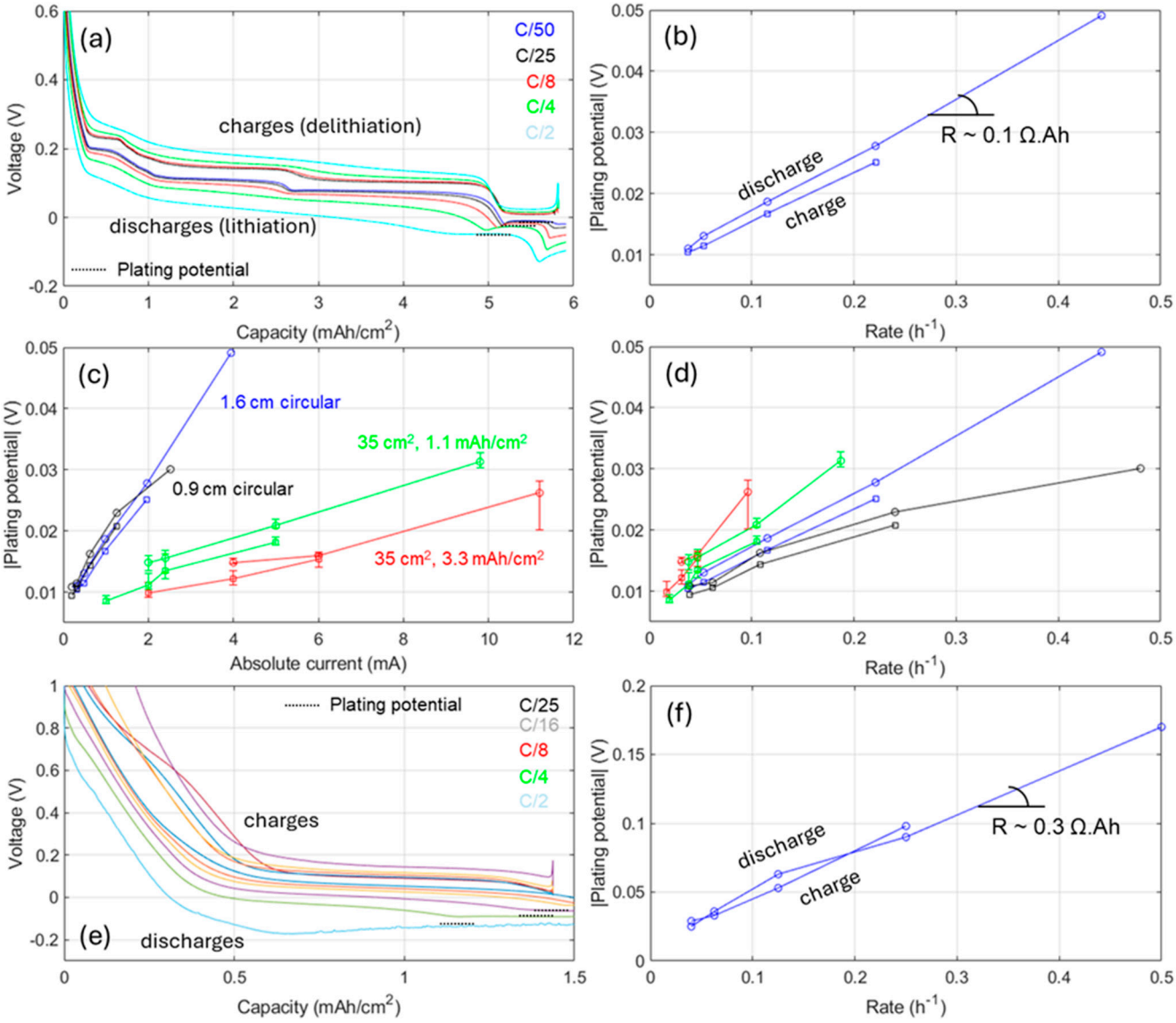

Figure 2. (**a**) Lithiation voltage vs. capacity curve for a 1.6 cm^2 graphite electrode vs. metallic lithium at different rates and (**b**) the evolution of the lithium plating/stripping potential as a function of the rate. Absolute lithium plating potential for 4 different sizes or loading vs. (**c**) the absolute current and (**d**) the rate. For the pouch cells, the plotted values correspond to the average for all five tested cells. The error bars indicate the measured spread of values. (**e**) Voltage vs. capacity curve for a 1.6 cm^2 hard carbon electrode vs. metallic sodium at different rates and (**f**) the evolution of the sodium plating/stripping potential as a function of the rate.

With the rate dependency established, the next key point was to determine whether this evolution is current or current density dependent. In other words, determine if that resistance would be the same for different electrode sizes or loadings. Figure 2c presents the evolution of the absolute plating potential in charge and discharge for three different sizes (0.9 cm and 1.5 cm diameter circular electrodes as well as 35 cm^2 7 × 5 cm ones) and three different loadings (5 mAh/cm^2 for the circular electrodes as well as 1.1 and 3.3 mAh/cm^2 for the rectangular 7 × 5 cm electrodes) for a graphite vs. metallic lithium cell. In Figure 2d, it is clear that while the plating potential vs. current curves were spread out, the one vs. rate were much closer with the 0.9 cm and 1.5 cm diameter electrodes, mostly overlapping, with the same being true for both loadings for the rectangular electrodes. The difference in slope between the two sets of data might have been induced by the fact that different graphites, separators, and electrolytes were. The plotted value for the 35 cm^2 electrodes corresponds to the average of the five tested cells with the error bars showcasing their spread. The results indicated that the voltages were very similar and that, therefore, the plating potential was consistent between cells. It must be noted that the response for the 0.9 cm electrode did not seem to follow the linear trend for the higher rates, which might be related to mass transport limitations. Future work will investigate the extent of the linear relationship using a three-electrodes setup to eliminate errors on overpotentials.

Figure 2e,f present the results for cells containing hard carbon and metallic sodium that also underwent discharges up to 130% of their nominal capacity. Contrary to the lithium plating, no dip then increase was observed, but the plating potential was still rate dependent. The plating that measured plating resistance was estimated to be three times higher than the lithium one at 0.3 Ω Ah, but the materials and electrolytes were different.

Based on the results obtained, a new RPT protocol was tested with a rate-dependent end-of-discharge cutoff voltage. For this preliminary work, the goal was not to go as low as possible but to demonstrate the concept. The cutoff voltages were chosen to progressively decrease from −5 mV to −115 mV when the rate increased from C/25 to 4C, as shown in Figure 3a. The new protocol was successful in allowing more complete discharges for higher rates with an increase in capacity of 20%, 33%, and 20% for 4C, 2C, and 1C, respectively. It must be noted that the 2C and 4C discharge might still be incomplete since no inflection point was reached at the end of discharge. Moreover, no electrochemical features associated with lithium plating were observed. However, since plating could still have happened locally, the rest cell voltages after discharge were investigated thoroughly, as the literature showed that the lithium stripping that would occur during rest has a distinguishable signature [9,37,40–42] with a plateau after around, at least, 15 min of rest. Figure 3b presents the differential voltage analysis, dV/dt, as a function of t for the rests measured after discharge. The evolution of the rests was found to be monotonic, and no plateau associated with plating was observed, even for the higher rates where the discharge was stopped more than 100 mV below the traditional cutoff. This confirms that the plating potential is indeed rate dependent and that discharges below 0 V for NE could be performed to extract more information. However, the full impact on rate capability and durability is yet to be assessed.

For demonstration purposes, the data obtained for the new RPT protocol were imported into the alawa toolbox [35]. In addition, a parameter allowing to vary the plating resistance was also implemented. In this example, the resistance was set to R_{li} = 33 mΩ Ah to match the voltage cutoff voltages on the modified RPT protocol. Figure 3c presents the results from a simulation similar to Figure 1 but with the new extended electrode. Because more data were acquired for the higher rates, the charges are more complete, and no lithium plating is predicted because the cutoff voltage is reached before the NE full lithiation and the plating initiation, as shown in Figure 3d. This exemplifies the necessity of this correction, as this behavior is much closer to real recent commercial cells where plating typically should not occur for charges at C/1 at room temperature.

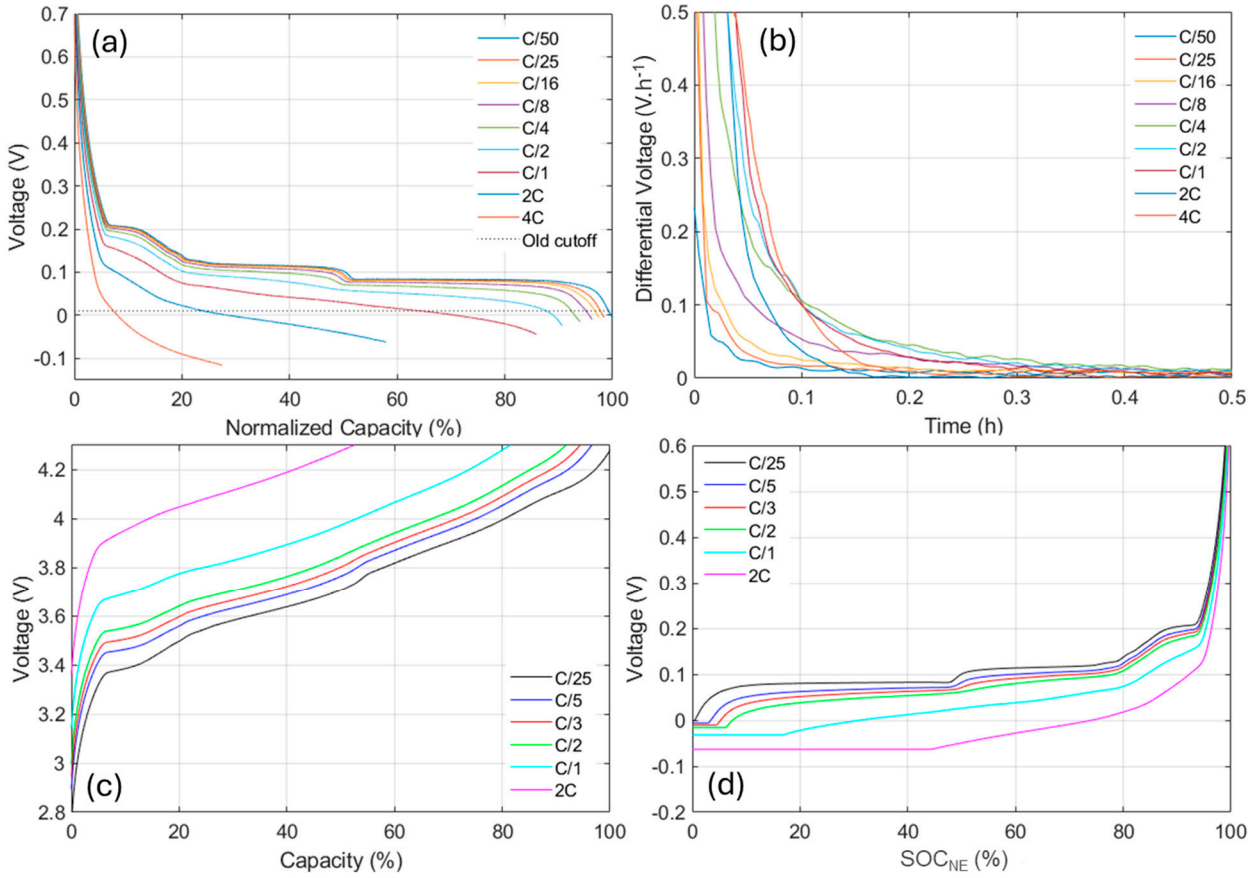

Figure 3. (**a**) Comparison of the lithiation voltage response for the new extended RPT schedule with (**b**) differential voltage vs. time curves for the rests after discharge. The dotted line represents the typical 10 mV cutoff. (**c**) Example of full-cell charging emulation at different rates with extended RPT and (**d**) the associated NE lithiation half-cell data used for the simulations.

4. Conclusions

To summarize, the results from this preliminary work established that the plating potential is rate dependent and that this can easily be taken into consideration to extend the potential window of electrodes during testing and to more accurately predict plating onset dynamically in battery models outside of equilibrium. While the voltage window needs to be extended to its maximum to avoid discontinuity in the simulations, our preliminary results showcased that discharging to more than 130% of the nominal capacity might induce some electrode degradation, which is counterproductive if the data are to be used as references in a model. Therefore, more work is needed to maximize data gathering while minimizing the induced degradation. Hopefully, a protocol can be defined to allow for the gathering of maximum data and estimate the plating resistance at the same time. However, that might not be an easy task, as it was also identified that the plating potential might be dependent on the type of carbon, electrolyte, or separators. This must, therefore, be investigated in more detail, along with the impact of temperature and other parameters, like pressure, before any generalization can be proposed for lithium- and sodium-ion batteries.

Author Contributions: Conceptualization, M.D.; methodology, M.D. and A.R.; software, M.D.; validation, M.D., D.B., A.G., and A.R.; formal analysis, M.D. and D.B.; investigation, M.D.; resources, M.D. and A.R.; data curation, M.D.; writing—original draft preparation, M.D.; writing—review and editing, M.D., D.B., A.G., and A.R.; visualization, M.D.; supervision, M.D. and A.R.; project administration, M.D. and A.R.; funding acquisition, M.D. and A.R. All authors have read and agreed to the published version of the manuscript.

Funding: This research was funded by ONR grant number N00014-20-1-2270 and the Faraday Institution (EP/S003053/1) via the LiSTAR project (FIRG058).

Data Availability Statement: The complete dataset will be made available after the completion of the full study. Preliminary data can be found here: doi:10.17632/98g66p2v9k.1. Additional data will be made available upon reasonable request.

Conflicts of Interest: The authors declare no conflicts of interest.

References

1. Vetter, J.; Novák, P.; Wagner, M.R.; Veit, C.; Möller, K.C.; Besenhard, J.O.; Winter, M.; Wohlfahrt-Mehrens, M.; Vogler, C.; Hammouche, A. Ageing mechanisms in lithium-ion batteries. *J. Power Sources* **2005**, *147*, 269–281. [CrossRef]
2. Agubra, V.; Fergus, J. Lithium Ion Battery Anode Aging Mechanisms. *Materials* **2013**, *6*, 1310–1325. [CrossRef] [PubMed]
3. Waldmann, T.; Hogg, B.-I.; Wohlfahrt-Mehrens, M. Li plating as unwanted side reaction in commercial Li-ion cells—A review. *J. Power Sources* **2018**, *384*, 107–124. [CrossRef]
4. Janakiraman, U.; Garrick, T.R.; Fortier, M.E. Review—Lithium Plating Detection Methods in Li-Ion Batteries. *J. Electrochem. Soc.* **2020**, *167*, 160552. [CrossRef]
5. Edge, J.S.; O'Kane, S.; Prosser, R.; Kirkaldy, N.D.; Patel, A.N.; Hales, A.; Ghosh, A.; Ai, W.; Chen, J.; Yang, J.; et al. Lithium ion battery degradation: What you need to know. *Phys. Chem. Chem. Phys.* **2021**, *23*, 8200–8221. [CrossRef]
6. Lin, X.; Khosravinia, K.; Hu, X.; Li, J.; Lu, W. Lithium Plating Mechanism, Detection, and Mitigation in Lithium-Ion Batteries. *Progr. Energy Combust. Sci.* **2021**, *87*, 100953. [CrossRef]
7. Paul, P.P.; McShane, E.J.; Colclasure, A.M.; Balsara, N.; Brown, D.E.; Cao, C.; Chen, B.R.; Chinnam, P.R.; Cui, Y.; Dufek, E.J.; et al. A Review of Existing and Emerging Methods for Lithium Detection and Characterization in Li-Ion and Li-Metal Batteries. *Adv. Energy Mater.* **2021**, *11*, 2100372. [CrossRef]
8. Tian, Y.; Lin, C.; Li, H.; Du, J.; Xiong, R. Detecting undesired lithium plating on anodes for lithium-ion batteries—A review on the in-situ methods. *Appl. Energy* **2021**, *300*, 117386. [CrossRef]
9. Chen, Y.; Torres-Castro, L.; Chen, K.-H.; Penley, D.; Lamb, J.; Karulkar, M.; Dasgupta, N.P. Operando detection of Li plating during fast charging of Li-ion batteries using incremental capacity analysis. *J. Power Sources* **2022**, *539*, 231601. [CrossRef]
10. Tanwar, M.; Bezabh, H.K.; Basu, S.; Su, W.N.; Hwang, B.J. Investigation of Sodium Plating and Stripping on a Bare Current Collector with Different Electrolytes and Cycling Protocols. *ACS Appl. Mater. Interfaces* **2019**, *11*, 39746–39756. [CrossRef]
11. Yang, X.-G.; Leng, Y.; Zhang, G.; Ge, S.; Wang, C.-Y. Modeling of lithium plating induced aging of lithium-ion batteries: Transition from linear to nonlinear aging. *J. Power Sources* **2017**, *360*, 28–40. [CrossRef]
12. Bohinsky, A.; Rangarajan, S.P.; Barsukov, Y.; Mukherjee, P. Preventing lithium plating under extremes: An untold tale of two electrodes. *J. Mater. Chem. A* **2021**, *9*, 17249–17260. [CrossRef]
13. Rangarajan, S.P.; Barsukov, Y.; Mukherjee, P.P. Anode potential controlled charging prevents lithium plating. *J. Mater. Chem. A* **2020**, *8*, 13077–13085. [CrossRef]
14. Von Lüders, C.; Keil, J.; Webersberger, M.; Jossen, A. Modeling of lithium plating and lithium stripping in lithium-ion batteries. *J. Power Sources* **2019**, *414*, 41–47. [CrossRef]
15. Carelli, S.; Bessler, W.G. Prediction of Reversible Lithium Plating with a Pseudo-3D Lithium-Ion Battery Model. *J. Electrochem. Soc.* **2020**, *167*, 100515. [CrossRef]
16. Li, Z.; Jian, Z.; Wang, X.; Rodriguez-Perez, I.A.; Bommier, C.; Ji, X. Hard carbon anodes of sodium-ion batteries: Undervalued rate capability. *Chem. Commun.* **2017**, *53*, 2610–2613. [CrossRef]
17. Iermakova, D.I.; Dugas, R.; Palacín, M.R.; Ponrouch, A. On the Comparative Stability of Li and Na Metal Anode Interfaces in Conventional Alkyl Carbonate Electrolytes. *J. Electrochem. Soc.* **2015**, *162*, A7060–A7066. [CrossRef]
18. Cohn, A.P.; Muralidharan, N.; Carter, R.; Share, K.; Pint, C.L. Anode-Free Sodium Battery through in Situ Plating of Sodium Metal. *Nano Lett.* **2017**, *17*, 1296–1301. [CrossRef]
19. Sarkar, S.; Lefler, M.J.; Vishnugopi, B.S.; Nuwayhid, R.B.; Love, C.T.; Carter, R.; Mukherjee, P.P. Fluorinated ethylene carbonate as additive to glyme electrolytes for robust sodium solid electrolyte interface. *Cell Rep. Phys. Sci.* **2023**, *4*, 101356. [CrossRef]
20. Hijazi, H.; Ye, Z.; Zhang, L.; Deshmukh, J.; Johnson, M.B.; Dahn, J.R.; Metzger, M. Impact of Sodium Metal Plating on Cycling Performance of Layered Oxide/Hard Carbon Sodium-ion Pouch Cells with Different Voltage Cut-offs. *J. Electrochem. Soc.* **2023**, *170*, 070512. [CrossRef]
21. Desai, P.; Abou-Rjeily, J.; Tarascon, J.-M.; Mariyappan, S. Practicality of methyl acetate as a co-solvent for fast charging Na-ion battery electrolytes. *Electrochim. Acta* **2022**, *416*, 140217. [CrossRef]
22. Zheng, Y.; Lu, Y.; Qi, X.; Wang, Y.; Mu, L.; Li, Y.; Ma, Q.; Li, J.; Hu, Y.-S. Superior electrochemical performance of sodium-ion full-cell using poplar wood derived hard carbon anode. *Energy Storage Mater.* **2019**, *18*, 269–279. [CrossRef]
23. Yan, L.; Zhang, G.; Wang, J.; Ren, Q.; Fan, L.; Liu, B.; Wang, Y.; Lei, W.; Ruan, D.; Zhang, Q.; et al. Revisiting Electrolyte Kinetics Differences in Sodium Ion Battery: Are Esters Really Inferior to Ethers? *Energy Environ. Mater.* **2022**, *6*, e12523. [CrossRef]
24. Bloom, I.; Jansen, A.N.; Abraham, D.P.; Knuth, J.; Jones, S.A.; Battaglia, V.S.; Henriksen, G.L. Differential voltage analyses of high-power, lithium-ion cells. 1. Technique and Applications. *J. Power Sources* **2005**, *139*, 295–303. [CrossRef]

25. Bloom, I.; Christophersen, J.; Gering, K. Differential voltage analyses of high-power, lithium-ion cells. 2. Applications. *J. Power Sources* **2005**, *139*, 304–313. [CrossRef]
26. Honkura, K.; Honbo, H.; Koishikawa, Y.; Horiba, T. State Analysis of Lithium-Ion Batteries Using Discharge Curves. *ECS Trans.* **2008**, *13*, 61–73. [CrossRef]
27. Dahn, H.M.; Smith, A.J.; Burns, J.C.; Stevens, D.A.; Dahn, J.R. User-Friendly Differential Voltage Analysis Freeware for the Analysis of Degradation Mechanisms in Li-Ion Batteries. *J. Electrochem. Soc.* **2012**, *159*, A1405–A1409. [CrossRef]
28. Dubarry, M.; Truchot, C.; Liaw, B.Y. Synthesize battery degradation modes via a diagnostic and prognostic model. *J. Power Sources* **2012**, *219*, 204–216. [CrossRef]
29. Birkl, C.R.; Roberts, M.R.; McTurk, E.; Bruce, P.G.; Howey, D.A. Degradation diagnostics for lithium ion cells. *J. Power Sources* **2017**, *341*, 373–386. [CrossRef]
30. Anseán, D.; Dubarry, M.; Devie, A.; Liaw, B.Y.; García, V.M.; Viera, J.C.; González, M. Operando lithium plating quantification and early detection of a commercial LiFePO 4 cell cycled under dynamic driving schedule. *J. Power Sources* **2017**, *356*, 36–46. [CrossRef]
31. Baure, G.; Dubarry, M. Synthetic vs. Real Driving Cycles: A Comparison of Electric Vehicle Battery Degradation. *Batteries* **2019**, *5*, 42. [CrossRef]
32. Dubarry, M.; Baure, G.; Anseán, D. Perspective on State-of-Health Determination in Lithium-Ion Batteries. *J. Electrochem. Energy Convers. Storage* **2020**, *17*, 044701. [CrossRef]
33. Dubarry, M.; Beck, D. Perspective on Mechanistic Modeling of Li-Ion Batteries. *Acc. Mater. Res.* **2022**, *3*, 843–853. [CrossRef]
34. Verbrugge, M.W.; Koch, B.J. The effect of large negative potentials and overcharge on the electrochemical performance of lithiated carbon. *J. Electroanal. Chem.* **1997**, *436*, 1–7. [CrossRef]
35. HNEI. Alawa Central. Available online: https://www.hnei.hawaii.edu/alawa (accessed on 2 November 2024).
36. Dubarry, M.; Baure, G. Perspective on Commercial Li-ion Battery Testing, Best Practices for Simple and Effective Protocols. *Electronics* **2020**, *9*, 152. [CrossRef]
37. Chen, Y.; Chen, K.-H.; Sanchez, A.J.; Kazyak, E.; Goel, V.; Gorlin, Y.; Christensen, J.; Thornton, K.; Dasgupta, N.P. Operando video microscopy of Li plating and re-intercalation on graphite anodes during fast charging. *J. Mater. Chem. A* **2021**, *9*, 23522–23536. [CrossRef]
38. Zhou, H.; Fear, C.; Carter, R.E.; Love, C.T.; Mukherjee, P.P. Correlating Lithium Plating Quantification with Thermal Safety Characteristics of Lithium-ion Batteries. *Energy Storage Mater.* **2024**, *66*, 103214. [CrossRef]
39. Wood, K.N.; Kazyak, E.; Chadwick, A.F.; Chen, K.H.; Zhang, J.G.; Thornton, K.; Dasgupta, N.P. Dendrites and Pits: Untangling the Complex Behavior of Lithium Metal Anodes through Operando Video Microscopy. *ACS Cent. Sci.* **2016**, *2*, 790–801. [CrossRef] [PubMed]
40. Schindler, S.; Bauer, M.; Petzl, M.; Danzer, M.A. Voltage relaxation and impedance spectroscopy as in-operando methods for the detection of lithium plating on graphitic anodes in commercial lithium-ion cells. *J. Power Sources* **2016**, *304*, 170–180. [CrossRef]
41. Petzl, M.; Danzer, M.A. Nondestructive detection, characterization, and quantification of lithium plating in commercial lithium-ion batteries. *J. Power Sources* **2013**, *254*, 80–87. [CrossRef]
42. Campbell, I.D.; Marzook, M.; Marinescu, M.; Offer, G.J. How Observable Is Lithium Plating? Differential Voltage Analysis to Identify and Quantify Lithium Plating Following Fast Charging of Cold Lithium-Ion Batteries. *J. Electrochem. Soc.* **2019**, *166*, A725–A739. [CrossRef]